nature photonics

ARTICLES

PUBLISHED ONLINE: 21 JUNE 2009 | DOI: 10.1038/NPHOTON.2009.98

Multispectral opto-acoustic tomography of deep-seated fluorescent proteins *in vivo*

Daniel Razansky[1]*, Martin Distel[2], Claudio Vinegoni[3], Rui Ma[1], Norbert Perrimon[4], Reinhard W. Köster[2] and Vasilis Ntziachristos[1]*

Fluorescent proteins have become essential reporter molecules for studying life at the cellular and sub-cellular level, re-defining the ways in which we investigate biology. However, because of intense light scattering, most organisms and tissues remain inaccessible to current fluorescence microscopy techniques at depths beyond several hundred micrometres. We describe a multispectral opto-acoustic tomography technique capable of high-resolution visualization of fluorescent proteins deep within highly light-scattering living organisms. The method uses multiwavelength illumination over multiple projections combined with selective-plane opto-acoustic detection for artifact-free data collection. Accurate image reconstruction is enabled by making use of wavelength-dependent light propagation models in tissue. By performing whole-body imaging of two biologically important and optically diffuse model organisms, *Drosophila melanogaster* pupae and adult zebrafish, we demonstrate the facility to resolve tissue-specific expression of eGFP and mCherrry fluorescent proteins for precise morphological and functional observations *in vivo*.

Fluorescence protein (FP) imaging is increasingly being used as a key technology allowing the comprehension of complex and diverse mechanisms in many areas of biology and medical research[1]. By allowing *in vivo* observation of multifactorial dynamic interactions, confocal and multiphoton tissue-sectioning microscopies have become the major means of FP visualization, radically changing biological understanding[2–4]. Despite significant technological progress[4–7], high-resolution imaging is limited by the interaction of photons with cellular interfaces and organelles, which results in high levels of photon scattering. Consequently, state-of-the-art intravital (*in vivo*) microscopy operates only at depths that are less than one transport mean free path length (MFPL) in tissue[8] (the distance it takes for light to become highly diffuse, typically between a few hundred micrometres and 1 mm). As a result, a significant amount of *in vivo* biological research revolves around the study of organisms that are virtually transparent, such as early-stage *Caenorhabditis elegans* or zebrafish (*Danio rerio*)[9], or uses highly invasive techniques such as the implementation of biocompatible windows to study activity deeper in the body[10]. Optical projection tomography (OPT)[11], selective-plane illumination microscopy (SPIM)[12] and ultramicroscopy[13] have been developed recently as alternative tomographic methods to confocal and nonlinear microscopy, but are also strongly limited by tissue scattering. They can be similarly applied to the imaging of naturally transparent live specimens, such as organisms at very early stages of development, or organisms and tissues chemically treated to remove scattering (when applied to dimensions of the order of one MFPL or larger), which applies therefore only to studies that can be performed post mortem.

The urgent need to improve *in vivo* visualization capacity in the post-genomic era has been recently outlined[14]. *In vivo* imaging beyond one transport MFPL can be used to follow cell motility and interaction or organ development and function within large tissue volumes over long periods of time[15]. Non-invasive high-resolution tomographic imaging of FPs in adult organisms and mice could therefore offer an important visualization tool for functional genomics and proteomics at different system levels, that is, from the cell to the organ. Such a capacity will also shift the paradigm of biological observations and accelerate discovery by enabling *in vivo* longitudinal observation of dynamic phenomena on the same growing or developing organism, thus minimizing the need for laborious histological examinations and large cohorts to obtain meaningful statistics. From high-throughput whole-body phenotyping and time-lapse imaging in adult model organisms to understanding signalling and interactions of tissues with drugs and environmental factors, visualization beyond the penetration limit of modern microscopy will open new pathways for biological discovery.

In this work we report on the visualization of fluorescent proteins well beyond the penetration limits of optical microscopy while preserving high sensitivity and spatial resolution. To achieve this, we have developed and implemented a selective-plane multispectral opto-acoustic tomography (MSOT) method based on ultrasonic detection of pressure waves generated by the absorption of pulsed light in elastic media. The amplitude of the broadband ultrasound waves, generated by the absorption of pulsed light by tissue chromophores[16], is processed tomographically to offer three-dimensional images of optical contrast reaching ultrasonic diffraction-limited resolution, not limited by the degree of light scattering. The ability to create images based on opto-acoustics has already been established in resolving vascular structures[17,18] and functional imaging in mice[19]. Applied in reflectance scanning mode, high-resolution functional photoacoustic microscopy[20] has also demonstrated the ability to image subcutaneous tumour angiogenesis and blood oxygen saturation in rats and humans at a depth of ~600 μm. In recent years, attention has also been given to resolving molecular contrast using fluorescent contrast agents[21], chromogenic assays[22] and nanoparticles[23].

[1]Institute for Biological and Medical Imaging, Technical University of Munich and Helmholtz Center Munich, Ingolstädter Landstraße 1, D-85764 Neuherberg, Germany, [2]Institute of Developmental Genetics, Helmholtz Center Munich, Ingolstädter Landstraße 1, D-85764 Neuherberg, Germany, [3]Center for Systems Biology, Massachusetts General Hospital and Harvard Medical School, Richard B. Simches Research Center, 185 Cambridge Street, Boston, Massachusetts 02114, USA, [4]Department of Genetics, Harvard Medical School and Howard Hughes Medical Institute, 77 Avenue Louis Pasteur, Boston, Massachusetts 02115, USA. *e-mail: dr@tum.de; v.ntziachristos@tum.de

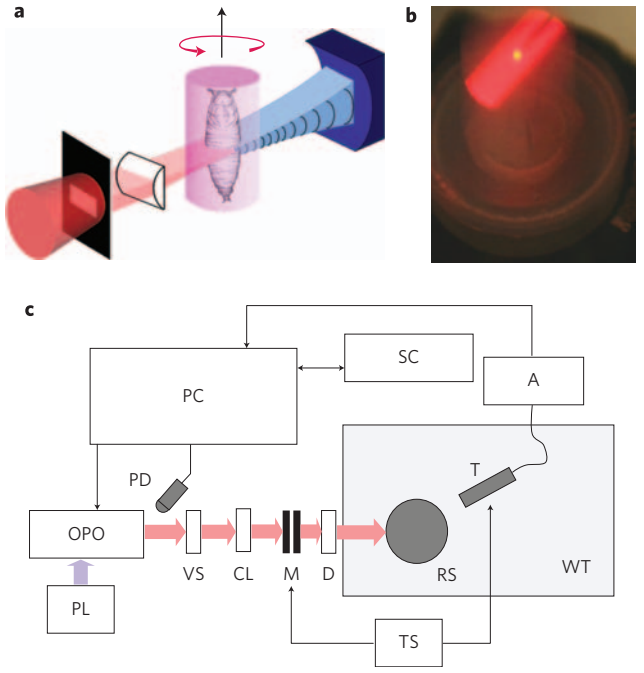

Figure 1 | Experimental setup of multispectral opto-acoustic tomography. **a**, Confocal illumination and detection scheme (red, illuminating light beam; blue, generated ultrasonic waves). **b**, Top-view photograph of the cylindrically focused beam passing through agar phantom with embedded *Drosophila* pupae. **c**, Schematic of the experimental setup. OPO, optical parametric oscillator; RS, rotation stage; SC, stage controller; VS, variable slit; CL, cylindrical lens; WT, water tank; D, engineered diffuser; T, ultrasonic transducer; M, mirror; TS, translation stage; PD, photodiode; PC, computer; A, amplifier; PL, pump laser.

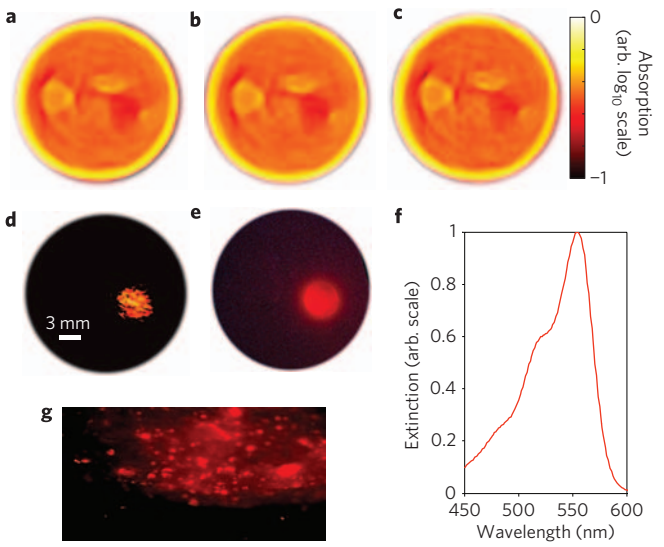

Figure 2 | Multispectral opto-acoustic imaging of tissue-mimicking phantom containing DsRed-expressing HeLa cells. a–c, Single-wavelength opto-acoustic images of the phantom acquired at 550 nm (**a**), 560 nm (**b**) and 570 nm (**c**). **d**, Spectrally resolved (MSOT) image of DsRed distribution in the phantom. **e**, Fluorescence image of dissected phantom at approximately the same imaging plane (red colour corresponds to the location of fluorescent cells). **f**, Extinction spectra of DsRed. **g**, Magnified image of phantom at the boundary of the area containing the DsRed cells.

In contrast to existing studies, we have established a multiprojection MSOT method that can volumetrically resolve FPs *in vivo* in small animals and tissues. By combining selective-plane illumination to minimize out-of-plane contributions and tomographic principles for image reconstruction, we demonstrate that it is possible to tune accurately the inversion process and detect specific FPs over non-specific background absorption with high sensitivity. In addition, the underlining anatomical images of the tissue are simultaneously provided. Applied to biological specimens, this technology extends fluorescence imaging to dimensions never visualized optically in the past, because it is capable of *in vivo* visualization of fluorescent proteins in intact model organisms at depth scales that are significantly larger than 1 mm, currently unattainable by other imaging techniques applied to living specimens, including confocal and multiphoton microscopies.

The experimental setup used nanosecond pulsed laser illumination at multiple wavelengths, which passed through a variable-slit aperture and focused, using a cylindrically focusing lens, onto the sample, creating a planar sheet of light (Fig. 1). The imaged objects were fixed on a rotation stage submerged into water to facilitate detection of acoustic signals. Opto-acoustic signals were recorded by a broadband ultrasonic transducer, cylindrically focused at the optical illumination plane (confocal arrangement). At each illumination wavelength and imaging height, the in-plane images were reconstructed using a filtered back-projection algorithm (see Methods for details on the experimental system and image reconstruction algorithms).

To confirm the basic ability of the method to detect fluorescent proteins over background absorption and quantify its performance, a cylindrical tissue-mimicking phantom (diameter, 1.9 cm; optical absorption coefficient, 0.3 cm^{-1}; scattering, 10 cm^{-1}) was generated by dissolving India ink and Intralipid in agar (see Supplementary information for a detailed description of phantom preparation). The phantom mimics the dimensions and average optical properties of mouse tissue at a wavelength of ~630 nm. Two 4-mm-diameter insertions were incorporated into the phantom. The first insertion contained stable transgenic HeLa cells (4×10^6 ml^{-1}) expressing a mitochondrial targeted DsRedT4 fluorescent protein variant mixed with a solution of Intralipid and ink similar to background. The second insertion (absorption coefficient, 0.6 cm^{-1}; scattering, 10 cm^{-1}) served as a control and contained a higher concentration of India ink but no fluorescent cells.

The principle of detection is based on differentiation of the absorption spectral signature of the protein over background tissue absorption by the analysis of multiwavelength data. Fluorescent proteins are excellent molecules for this role compared to other chromophoric substances such as India ink, because they exhibit a steep declining absorption slope at lower energies, which can easily be detected spectroscopically, as shown in Fig. 2f, by taking measurements at multiple wavelengths. Although single-wavelength images only reveal the highly absorbing control insertion and some phantom heterogeneities (Fig. 2a–c), the non-specific contrast from the insertion containing DsRed-expressing cells is barely visible. Nevertheless, multiwavelength processing of the images on a per-pixel basis (see Methods) renders high contrast from the FP-expressing cells with a contrast-to-noise ratio (CNR) of 32, while suppressing other non-specific contrast (Fig. 2d). The results show excellent agreement with the epifluorescence image shown in Fig. 2e, obtained after phantom sectioning to validate the tomographic images of the intact phantom.

To investigate the *in vivo* capacity of the method to image tissues beyond the limits of modern microscopy, the zebrafish and *Drosophila melanogaster* (fruit fly) were selected as the imaging targets, partly because these organisms are extensively used in various fields of genetics and other areas of modern biology. By extending non-invasive fluorescence imaging of optically transparent organisms in early development stages to imaging opaque

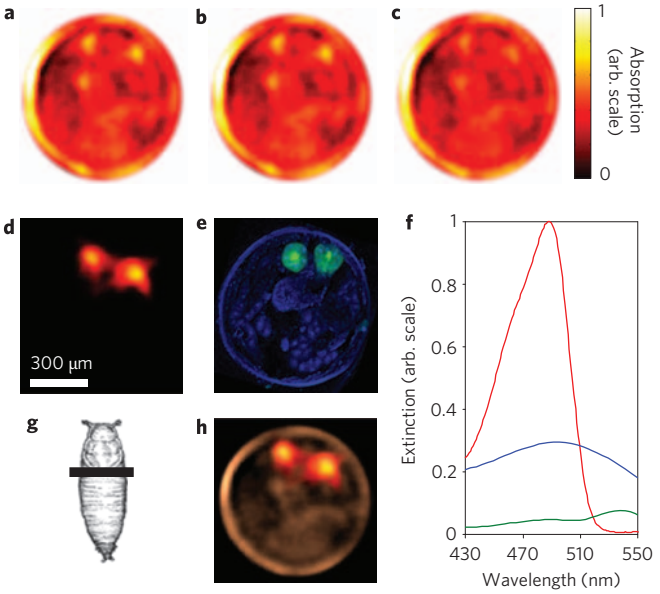

Figure 3 | Imaging of eGFP distribution in *Drosophila melanogaster* pupa. **a**–**c**, Opto-acoustic images acquired at 488 nm (**a**), 498 nm (**b**) and 508 nm (**c**). **d**, Spectrally resolved (MSOT) image of eGFP distribution in an intact pupa. **e**, Corresponding histology of DAPI-stained pupa at approximately the same imaging plane (green colour corresponds to GFP-expressing salivary glands). **f**, Extinction spectra of eGFP (red) along with measured absorption of pupa case (blue) and fat areas (green). **g**, Imaging plane. **h**, Overlay between the image at 508 nm (**c**) and the spectrally resolved image.

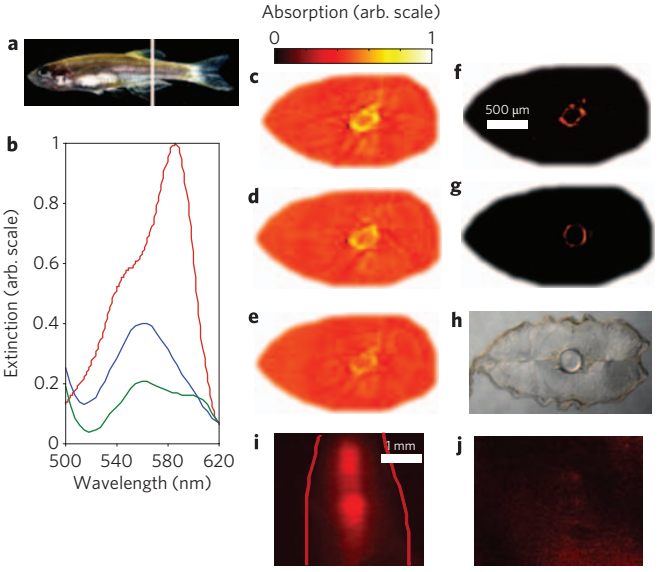

Figure 4 | Imaging of mCherry distribution in the vertebral column of an adult zebrafish. **a**, Location of the imaging plane. **b**, Extinction spectra of mCherry (red curve) and the intrinsic background (vertebral column, blue; muscles, green). **c**–**e**, Opto-acoustic images acquired at 587 nm (**c**), 597 nm (**d**) and 607 nm (**e**). **f**, Spectrally resolved image of mCherry distribution in an intact animal. **g**, Histological epifluorescence image of dissected tissue at approximately the same imaging plane (red colour corresponds to mCherry-expressing vertebral column). **h**, Regular histological section. **i**, Epifluorescence image of a living zebrafish. Red curves show the surface outline. **j**, Coronal confocal image at a depth of ~500 μm from the surface. A juvenile two-month-old zebrafish was used in this case (short axis thickness of ~1 mm in the imaged area).

organisms through adulthood, several dynamic aspects of molecular and cellular mechanisms of disease aetiology and progression, aging and the effects of environmental factors may be studied *in vivo* in an intact specimen. Furthermore, the large number of FPs available have provided powerful tools for mechanistic and functional genetic research, and many transgenic models expressing these genetic fluorescent markers in a cell-type-specific manner have been established to investigate cellular and sub-cellular function.

Imaging results from a *Drosophila melanogaster* pupa are presented in Fig. 3. In this case, a Gal-4/UAS system was used to specifically express eGFP (enhanced green fluorescent protein) in the salivary glands of the fly pupae (see Supplementary information for details). The imaging plane was located in the posterior part of the salivary glands area, as shown in Fig. 3 g. In this pupal stage, the *Drosophila* exhibits significant scattering[25] and is not accessible through its intact case by conventional fluorescent microscopy. The opto-acoustic images at three representative wavelengths are shown in Fig. 3a–c. The pupal case is readily identified in those images as having rather high optical absorption compared to internal structures. The various fatty structures are also clearly visualized. As in the previous imaging sessions, despite their strong eGFP expression, the salivary glands are not clearly distinguishable on single-wavelength images due to other non-specific background absorption. Figure 3f shows the spectral response of the pupal tissue as calculated by corresponding multiwavelength opto-acoustic measurements. After spectral processing, the salivary glands can be accurately visualized as shown in Fig. 3d,h. The corresponding histological section at approximately the same imaging plane is shown in Fig. 3e and is in good agreement with the reconstruction. The in-plane spatial resolution of opto-acoustic images is mainly determined by the effective bandwidth of the ultrasonic detector (20 MHz), leading to ~38 μm diffraction limited (half-wavelength) resolution in water. The vertical resolution was limited by the focal width of the ultrasonic detector to 150 μm.

To demonstrate the ability of the system to image through larger dimensions, we imaged adult zebrafish. Figure 4 shows results from a transgenic three-month old zebrafish in which the Gal-4/UAS system was used to express the mCherry FP in the vertebral column (see Supplementary information for details). This transgenic strain was chosen because the vertebral column represents one of the deeper structures in the highly scattering adult trunk and thus provides a significant imaging challenge. The specimen, measuring 2.5×4 mm^2 (see image cross-section in Fig. 4a), was held in the imaging setup by an agar phantom. Illumination was performed at multiple wavelengths, targeting the steep declining slope of the mCherry extinction spectra shown in Fig. 4b. Opto-acoustic images of the mCherry-expressing zebrafish at three representative wavelengths are shown in Fig. 4c–e and, as expected, exhibit strong contrast from varying tissue absorption in the vertebral column and surrounding structures. Similarly, spectral decomposition accurately resolves the location of mCherry expression in the intact animal (Fig. 4f). Subsequent histological sectioning (Fig. 4h) and epifluorescence image recording of tissue sections (Fig. 4g) demonstrated high congruence between *in vivo* and *ex vivo* images from the animal. The MSOT images provided an in-plane spatial resolution of less than 40 μm, as can be elucidated from the thickness of the fluorescent ring-like structure of the vertebral column in Fig. 4f. This spatial resolution can be substantially improved by using ultrasonic detectors with larger bandwidth. There is no methodology currently available that allows visualization of reporter molecules at these resolutions and these dimensions. Existing microscopy methods are mostly limited by resolution and SNR degradation due to light diffusion beyond depths of ~500 μm in scattering tissue. For comparison, we also provide an image of a juvenile (one-month-old) zebrafish using confocal

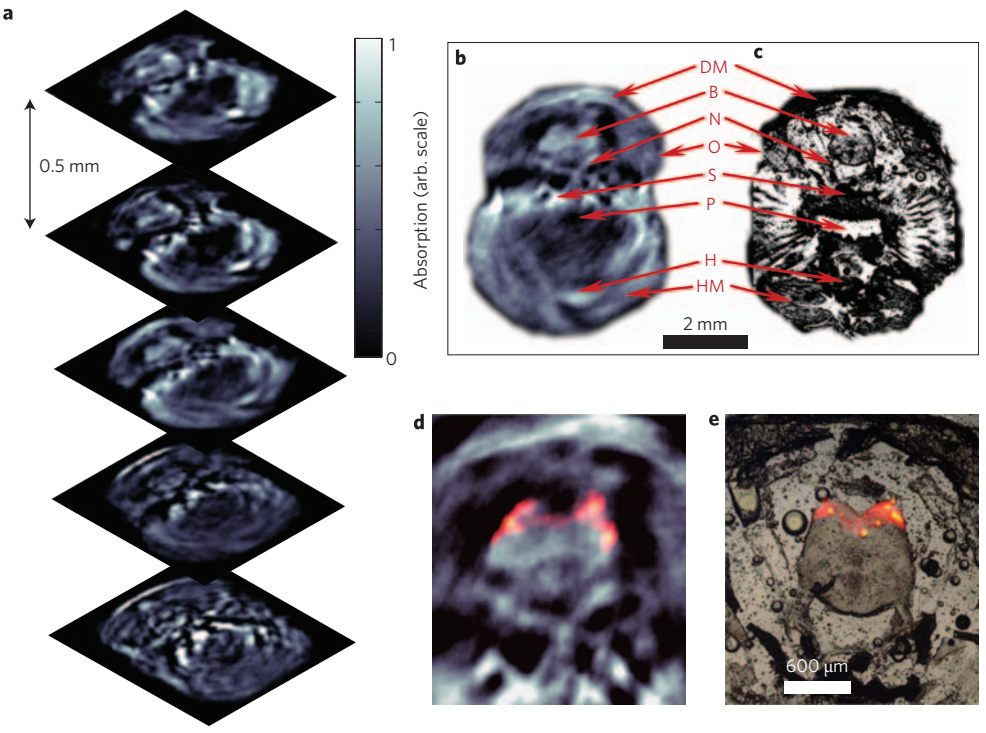

Figure 5 | Three-dimensional *in vivo* imaging through the brain of an adult (six-month-old) mCherry-expressing transgenic zebrafish. a, Five transverse opto-acoustic imaging slices through the hindbrain area at the level of crista cerebellaris of a living zebrafish taken at 585 nm. **b**,**c**, Example of an imaged slice (**b**) and its corresponding histological section in inverted colours (**c**). DM, dorsal fin musculature; B, hindbrain; N, lateral line nerve; O, operculum; S, skull bones; P, pharynx; H, heart; HM, hypobranchial musculature. **d**, MSOT image of the brain (enlarged) with mCherry expression shown in colour. **e**, Corresponding fluorescent histology of a dissected fish at the hindbrain level.

microscopy in Fig. 4j. Even though the cross-section here measures only ~1–2 mm as compared to 2.5–4 mm as imaged by MSOT, the confocal microscopy cannot image through the highly scattering juvenile zebrafish while an additional epifluorescence image (Fig. 4i) shows that the fluorescent vertebral column exhibits a highly diffusive appearance through 1–2 mm of tissue. Although multiphoton microscopy could possibly penetrate slightly deeper, it would also be limited by this light diffusion at about one transport MFPL, that is, <1 mm in scattering tissue.

To further showcase the MSOT capacity of performing three-dimensional *in vivo* scans we also imaged through the head of an adult (six-month-old) mCherry-expressing transgenic zebrafish (see Supplementary Information for details) with a cross-sectional diameter of ~6 mm. To guarantee survival, the fish was attached to the rotation stage by partially embedding it into modelling clay so that the upper parts including the head and gills were exposed to the anaesthetic solution (Tricaine) in the imaging tank. The fish fully recovered from the *in vivo* imaging sessions. The imaging results, shown in Fig. 5, demonstrate the ability of the process to reveal many morphological features, as is evident from Fig. 5a,b, supported by the corresponding histology (Fig. 5c). Moreover, multispectral reconstructions accurately resolved FP expression in the hindbrain of an intact living animal (Fig. 5d), in high congruence with the corresponding epifluorescence images of the dissected brain (Fig. 5e).

The ability to optically interrogate and visualize intact organisms beyond the limits of microscopy is of great importance in the post-genomic era for accelerating the study of genomics and proteomics. This work reports on the development of multiprojection multispectral opto-acoustic tomography (MSOT) for imaging biological organisms, and discusses its previously undocumented capacity for effectively detecting FPs in tissues, *in vivo*. The method was found to be capable of offering a new generation of biological imaging by visualizing optical reporter molecules deep inside the body of mature organisms with high (mesoscopic) resolution, while simultaneously providing the necessary reference anatomical images. A particular strength of the technology is its ability to scale with different tissue sizes. Imaging of a zebrafish up to 6 mm thick was shown. However, as demonstrated in phantom experiments, several centimetres of penetration with nearly the same resolution can be achieved, particularly when using near-infrared light. Indeed, many relevant biological samples and model organisms (such as worms, developing and adult insects, and vertebrates including small mammals and their extremities) have sizes lying in this range and could therefore be visualized.

The phantom measurements of Fig. 2 allow for the calculation and prediction of the detection limits of the current system. To achieve this, we performed a theoretical analysis to translate the system noise and signals detected from known volumes and cell populations to predict signals from different volumes and cell numbers of interest. The method uses an analytical solution of optical and acoustic propagation as well as target size and depth and yields, as recently described in ref. 24, a nonlinear dependence of signal strength with target volume. According to the spatio-temporal characteristics of the ultrasonic detector, the model assumed that the effective volume in the phantom of Fig. 2, from which the individual opto-acoustic signals were detected, contained on average $\sim 10^4$ cells and assumed a minimum detection limit corresponding to a CNR of 5 (that is, CNR < 5 does not constitute detection). In this case, the minimal detectable number of cells was found to be $\sim 10^3$. It was further calculated that, for achieving single cell detection sensitivity, the SNR of the system would need to be improved by a factor of ~2500, which corresponds to an equivalent increase of the signal or reduction of the noise floor by a factor of $\sqrt{2500} = 50$ (in rms voltage terms). Such an improvement is technically feasible and can be achieved by a combination of using

detectors of higher sensitivity, averaging over longer periods of time, or using larger arrays of detectors in parallel.

Multiwavelength imaging combined with selective-plane illumination offers the possibility of improving contrast, reducing out-of-plane and other imaging artifacts (see, for example, Fig. 3), as well as simultaneously resolving multiple FPs, dyes and other chromophores. In the applications shown, no photobleaching effects were observed, because the method operates with significantly less power per unit volume than that achieved with focused light, as in confocal microscopy. Although the spatial resolution in these studies was ~38 μm, broadband acoustic detectors constructed in arrays may lead to superior resolution and also offer real-time imaging capability, which is the goal of the next-generation setup. One important issue to be addressed regarding the accuracy of multispectral reconstruction is the wavelength dependence of the light distribution in tissue. As the MSOT method proposed herein capitalizes on the steep changes in absorption spectra of FPs in the vicinity of their excitation wavelength, it only needs very narrow spectral bands to operate efficiently (of the order of 30 nm). Within this spectral region the scattering properties of even very diffuse tissues are not expected to differ by more than 10% (assuming scattering is normally inversely proportional to the square of the wavelength), leading to corresponding fluence changes of less than 5%, as can be calculated by the light diffusion equation. However, if scattering variations in certain applications are higher, then correction on the data could be applied by corresponding adjustment of the photon diffusion model used to account for wavelength-dependent light propagation differences in the tissues due to scattering. In addition, because contrast is calculated in the spectral analysis on a relative per voxel basis, there is also low sensitivity to spatially varying scattering. Therefore, in contrast to conventional opto-acoustic imaging, MSOT is not affected significantly by possible scattering heterogeneity within the tissues or wavelengths used.

In comparison, surface-limited fluorescence microscopy methods or those applied to transparent or post mortem to chemically treated samples achieve better spatial resolution but offer penetration depths limited to less than one MFPL[25], that is, ~1 mm in the case of opaque living tissue. It is also possible to perform optical tomography through entire mice with high sensitivity, but low resolution[8,26] (~1 mm or worse). In contrast, selective-plane MSOT offers an imaging platform that is not limited by light diffusion and can achieve a penetration from several millimetres to potentially centimetres with a resolution that can vary practically in the range 20–100 μm. Importantly, the resolution achieved remains constant as a function of depth and depends only on the ultrasonic detector characteristics, that is, on bandwidth and sensitivity, as well as on the overall SNR achieved. MSOT therefore fills a significant area in biological imaging that goes well beyond the penetration limit of modern microscopy and could become the method of choice in studying signalling pathways and gene expression, morphogenesis, disease progression and many other targeted mechanisms through whole bodies of opaque living organisms and animals. It may not only significantly enhance the usefulness of currently existing transgenic FP lines, but may even call for the development of more reporters and probes that could tag, with higher flexibility, development, disease and aging-related processes.

Methods

Experimental setup and data acquisition. The schematic of the experimental setup is shown in Fig. 1c. It uses an optical parametric oscillator (OPO) based laser (MOPO series, Spectra Physics Inc.), tunable in the visible and near-infrared region (430–1,800 nm) and capable of producing 8-ns pulses with a repetition frequency of 30 Hz. The imaged objects were fixed on the rotation stage, controlled by a stage controller (ESP-3000, Newport Corp.). The laser beam was passed through a variable-slit aperture, and focused using a cylindrically focusing lens onto a sample submerged in water, thus creating a planar sheet of light. Before entering the water tank, the beam was further homogenized in the imaged (horizontal) plane using a diffuser to reduce the effects associated with hot spots and other beam instability artifacts. Maximal light intensity at the surface of the imaged objects was ~5 mW mm^{-2}. The geometric focal line was extended for ~2–3 mm into the scattering object to allow maximal possible confinement of a planar light sheet within the acoustic detection plane (image plane). This kind of selective-plane illumination strategy is especially useful in cases where the studied organism presents high absorption contrast between different structures. This is because, for the first one or two millimetres, the light is only partially diffused as it passes through the scattering object, thus, signals coming from 'out-of-focus plane' absorptive structures are minimized. Each imaged object was illuminated by up to seven wavelengths spaced by 10 nm and located near the peak excitation of the particular FP being imaged; however, a minimum of three wavelengths are normally required for efficient spectral decomposition. Broadband ultrasonic transducers (Models V382 and V319, Olympus-Panametrics, 100% bandwidth, central frequencies 3.5 and 15 MHz, respectively), cylindrically focused at the optical illumination plane (confocal arrangement), were used to detect the opto-acoustic signals. The V382 transducer was used for phantom measurements while the V319 model served in other high-resolution *in vivo* experiments. The samples were rotated 360° with 3° steps to enable in-plane two-dimensional image reconstruction. Three-dimensional data acquisition was enabled by means of vertical scanning of both illumination and detection planes by mounting the transducer and a 45°-angled mirror onto a vertical translational stage. The recorded time-resolved signals were amplified, digitized and averaged by an embedded oscilloscope PCI card at 100 Msps (NI PCI-5122, National Instruments Corp.) with 14-bit resolution. To further reduce beam instability artifacts and increase the accuracy of multispectral reconstructions, a photodiode was used to detect pulse energy and all recorded signals were normalized with the actual light energy on a per-pulse basis. Planar image data acquisition normally took ~2 min at each wavelength.

Image reconstruction. A filtered backprojection algorithm[27] was used to reconstruct the detected opto-acoustic responses. Two-dimensional single-wavelength image reconstruction was carried out on a dual-core Pentium IV 3.2 GHz processor with 2 GB RAM, and typically required ~3 s on a 200 × 200 mesh. Because the raw opto-acoustic signals represent a combined contribution of light fluence and optical absorption, to extract more accurate optical absorption data it might be necessary to normalize the images by the light distribution in the object. It was, however, found that for *Drosophila* and zebrafish, due to their relatively small size, normalization for light distribution was not critical for the quality of the reconstructed images. This is because, in the range considered, the signal drop of the light sheet is not significant (less than an order of magnitude) so it does not significantly affect image quality through SNR deterioration. Nevertheless, correction for light distribution is essential for the 1.9-cm-diameter phantom to obtain contrast from the deep structures[28]. To facilitate the correction, we represent the initially reconstructed opto-acoustic image as a product between optical absorption distribution $\mu_a(\boldsymbol{r})$ and local light fluence $U(\boldsymbol{r})$. The latter is calculated using a finite-element method (FEM) solution to the light diffusion equation

$$\nabla^2 U(\boldsymbol{r}) - k^2 U(\boldsymbol{r}) = -q_0$$

where $k = \sqrt{3\mu_a(\mu_a + \mu_a')}$. The light source term q_0 is assigned onto the phantom boundary, directly extracted from the opto-acoustic image. For first-order correction, we further assume that the phantom has homogeneous a priori known background optical properties. The average background properties of an object can in principle be approximately measured by comparing the magnitude of the surface opto-acoustic response to the one recorded from a calibrated object with known optical properties. Subsequently, the initial images at each wavelength are normalized by the calculated light distribution to obtain quantified optical absorption data on a per-pixel basis. In cases with a highly heterogeneous background with unknown optical properties, iterative normalization methods have been suggested for planar boundary two-dimensional configurations[29], and were recently extended to three dimensions by iteratively feeding data from a segmented opto-acoustic image into the FEM-based light diffusion model[30].

The correct location and concentration of FPs was resolved by spectral processing of opto-acoustic images[21,31] obtained at n discrete wavelengths $\lambda_1, \ldots, \lambda_n$. As mentioned, opto-acoustic measurements were taken in control animals containing no FPs to establish the spectral behaviour of the background absorption. It was subsequently assumed that every pixel k in the opto-acoustic image represents a combined contribution of the FP and the background. This can be written in the form of N linear equations:

$$\mu_a^k(\lambda_m) = \alpha_b(\lambda_m)c_b^k + \alpha_{FP}(\lambda_m)c_{FP}^k, \quad m = 1, \ldots, N$$

where $\mu_a^k(\lambda)$ is the reconstructed wavelength-dependent absorption in pixel k, $\alpha_b(\lambda)$ and $\alpha_{FP}(\lambda)$ are the molar extinction spectra of the FP and the background, and c_b^k and c_{FP}^k are the corresponding concentrations. Using the measured total absorption values and the known spectra for the measured wavelengths, the concentrations c_{FP}^k of the FP and the background c_b^k are subsequently reconstructed from the above linear equations on a per-pixel basis using a linear regression method. It should be noted that, although $\alpha_{FP}(\lambda)$ and c_{FP}^k represent the actual molar extinction coefficient of the FP and its concentration, the measured background spectra $\alpha_b(\lambda)$ and the extracted

values of the concentration c_b^k have arbitrary scale values and only their product $\alpha_b(\lambda)c_b^k$ has a real physical interpretation. Additional spectral contributions can be introduced by simply adding new terms to the spectral equations.

Received 27 November 2008; accepted 20 May 2009; published online 21 June 2009

References

1. Giepmans, B. N. G., Adams, S. R., Ellisman, M. H. & Tsien, R. Y. The fluorescent toolbox for assessing protein location and function. *Science* **312,** 217–224 (2006).
2. Lichtman, J. W. & Conchello, J. A. Fluorescence microscopy. *Nature Methods* **2,** 910–919 (2005).
3. Conchello J. A. & Lichtman, J. W. Optical sectioning microscopy. *Nature Methods* **2,** 920–931 (2005).
4. Bahlmann, K. *et al*. Multifocal multiphoton microscopy (MMM) at a frame rate beyond 600 Hz. *Opt. Express* **15,** 10991–10998 (2007).
5. Minsky, M. Microscopy apparatus. US patent 3,013,467 (1961).
6. Denk, W., Strickler, J. H. & Webb, W. W. 2-photon laser scanning fluorescence microscopy. *Science* **248,** 73–76 (1990).
7. Helmchen, F. & Denk, W. Deep tissue two-photon microscopy. *Nature Methods* **2,** 932–940 (2005).
8. Ntziachristos, V., Ripoll, J., Wang, L. H. V. & Weissleder, R. Looking and listening to light: the evolution of whole-body photonic imaging. *Nature Biotechnol.* **23,** 313–320 (2005).
9. Hove, J. R. *et al*. Intracardiac hemodynamics are an essential epigenetic factor for embryonic cardiogenesis. *Nature* **421,** 172–177 (2003).
10. Jain, R. K., Munn, L. L. & Fukumura, D. Dissecting tumor pathophysiology using intravital microscopy. *Nature Rev. Cancer* **2,** 266–276 (2002).
11. Sharpe, J. *et al*. Optical projection tomography as a tool for 3D microscopy and gene expression studies. *Science* **296,** 541–545 (2002).
12. Huisken, J. *et al*. Optical sectioning deep inside live embryos by selective plane illumination microscopy. *Science* **305**, 1007–1009 (2004).
13. Dodt, H. U. *et al*. Ultramicroscopy: three-dimensional visualization of neuronal networks in the whole mouse brain. *Nature Methods* **4,** 331–336 (2007).
14. Editorial. Geneticist seeks engineer: must like flies and worms. *Nature Methods* **4,** 463 (2007).
15. Schroeder, T. Imaging stem-cell-driven regeneration in mammals. *Nature* **453,** 345–351 (2008).
16. Gusev, V. E. & Karabutov, A. A. *Laser Optoacoustics* (*American Institute of Physics*, 1993).
17. Zhang, E. Z., Laufer, J. G., Pedley, R. B. & Beard, P. C. *In vivo* high-resolution 3D photoacoustic imaging of superficial vascular anatomy. *Phys. Med. Biol.* **54,** 1035–1046 (2009).
18. Lao, Y., Xing, D., Yang, S. & Xiang, L. Noninvasive photoacoustic imaging of the developing vasculature during early tumor growth. *Phys. Med. Biol.* **53,** 4203–4212 (2008).
19. Wang, X. *et al*. Noninvasive laser-induced photoacoustic tomography for structural and functional *in vivo* imaging of the brain. *Nature Biotechnol.* **21,** 803–806 (2003).
20. Zhang, H. F., Maslov, K., Stoica, G. & Wang, L. V. Functional photoacoustic microscopy for high-resolution and noninvasive *in vivo* imaging. *Nature Biotechnol.* **24,** 848–851 (2006).
21. Razansky, D., Vinegoni, C. & Ntziachristos, V. Multispectral photoacoustic imaging of fluorochromes in small animals. *Opt. Lett.* **32,** 2891–2893 (2007).
22. Li, L., Zemp, R. J., Lungu, G., Stoica, G. & Wang, L. V. Photoacoustic imaging of lacZ gene expression *in vivo*. *J. Biomed. Opt.* **12,** 020504 (2007).
23. De La Zerda, A. *et al*. Carbon nanotubes as photoacoustic molecular imaging agents in living mice. *Nature Nanotechnol.* **3,** 557–562 (2008).
24. Razansky, D., Baeten, J. & Ntziachristos, V. Sensitivity of molecular target detection by multispectral optoacoustic tomography (MSOT). *Med. Phys.* **36,** 2891–2893 (2009).
25. Vinegoni, C., Pitsouli, C., Razansky, D., Perrimon, N. & Ntziachristos, V. *In vivo* imaging of *Drospophila melanogaster* pupae with mesoscopic fluorescence tomography. *Nature Methods* **5,** 45–47 (2008).
26. Ntziachristos, V., Tung, C.-H., Bremer, C. & Weissleder, R. Fluorescence molecular tomography resolves protease activity *in vivo*. *Nature Med.* **8,** 757–760 (2002).
27. Xu, M. & Wang, L. V. Universal back-projection algorithm for photoacoustic computed tomography. *Phys. Rev. E* **71,** 016706 (2005).
28. Razansky, D. & Ntziachristos, V. Hybrid photoacoustic fluorescence molecular tomography using finite-element-based inversion. *Med. Phys.* **34,** 4293–4301 (2007).
29. Cox, B. T., Arridge, S. R., Kostli, K. P. & Beard, P. C. 2D quantitative photoacoustic image reconstruction of absorption distributions in scattering media using a simple iterative method. *Appl. Opt.* **45,** 1866–1875 (2006).
30. Jetzfellner, T. *et al*. Iterative optoacoustic image normalization in non-uniform illumination configurations. *Appl. Phys. Lett.* **95,** (2009) (in the press).
31. Laufer, J. G., Delpy, D. T., Elwell, C. E. & Beard, P. C. Quantitative spatially resolved measurement of tissue chromophore concentrations using photoacoustic spectroscopy: application to the measurement of blood oxygenation and haemoglobin concentration. *Phys. Med. Biol.* **52,** 141–168 (2007).

Acknowledgements

D.R. acknowledges financial support by the Deutsche Forschungsgemeinschaft (DFG) research grant RA 1848/1-1. M.D. is a fellow of the Studienstiftung des deutschen Volkes. R.W.K. is supported by a BioFuture Award Grant (0311889) of the German Ministry for Education and Research (BMBF). We thank R. Jagasia for providing Hela mitodsRed cells.

Additional information

Supplementary information accompanies this paper at www.nature.com/naturephotonics. Reprints and permission information is available online at http://npg.nature.com/reprintsandpermissions/. Correspondence and requests for materials should be addressed to D.R. and V.N.